Hydrostatic pressure effects on the electrical transport properties of $Pr_{0.5}Sr_{0.5}MnO_3$

F. J. Rueckert,[1,][*] M. Steiger,[1] B. K. Davis,[1,2] T. Huynh,[3] J. J. Neumeier,[3] and M. S. Torikachvili[1]

[1]*Department of Physics, San Diego State University, San Diego, California 92182, USA*
[2]*Quantum Design, 6325 Lusk Boulevard, San Diego, California 92121, USA*
[3]*Department of Physics, Montana State University, Bozeman, Montana 59717, USA*

We studied single-crystalline $Pr_{0.5}Sr_{0.5}MnO_3$ by means of measurements of magnetic susceptibility and specific heat at ambient pressure (P) and electrical resistivity (ρ) in hydrostatic pressures up to 2 GPa. This material displays ferromagnetic (FM) order, with Curie temperature $T_C \approx 255$ K. A crystallographic transformation from $I4/mcm$ to $Fmmm$ is accompanied by the onset of antiferromagnetism (AFM), with Néel temperature $T_N \approx 161$ K. The effect of pressure is to lower T_C and to raise T_N at the approximate rates of −3.2, and 14.2 K/GPa, respectively. Although the value of T_N increases with P, due to the enhancement of the superexchange interactions, the AFM-$Fmmm$ state is progressively suppressed, as pressure stabilizes the FM-$I4/mcm$ phase to lower temperatures. The ρ vs T data suggest that the AFM phase should be completely suppressed near 2.4 GPa.

PACS number(s): 71.30.+h, 75.47.Lx, 62.50.−p

I. INTRODUCTION

The interplay between the magnetic and crystallographic structures in the perovskite manganites of general composition $R_{1-x}A_x MnO_3$, where R is a trivalent rare earth ion and A is a divalent alkaline element, results in a number of interesting features, including remarkable magnetic and electronic behaviors, e.g., colossal magnetoresistance (CMR)[1,2] and charge order.[3] In light of the ability to tune these properties through experimental parameters, as, for example, composition, temperature (T), magnetic field (H), etc., it is tempting to consider these materials for a number of technological applications.[4–6] A charge-ordered insulating state is frequently observed below a characteristic temperature T_{co} in the manganites at half-doping level, i.e., when divalent A substitutes half of trivalent R.[6,7] The regular arrangement of Mn^{3+} and Mn^{4+} ions, first described by Goodenough as charge ordering,[3] sets in at T_{co}, as long range Coulomb interactions overcome the kinetic energy of charge carriers, inhibiting the double-exchange mechanism.[8]

Charge order and CMR are electronic phenomena originating from the interaction of charge carriers with both Mn^{3+} and Mn^{4+} ions and lattice distortions. Electronic and magnetic properties can be further affected by hole doping.[9] Electrical conductivity in these materials is sustained by a double-exchange mechanism as proposed by Zener,[10] in which charge flows as electrons hop between neighboring Mn ions with parallel spins along the $Mn^{3+}-O-Mn^{4+}$ bonds,[11] therefore providing coupling between electrical conductivity and spin dynamics.

The $Pr_{0.5}Sr_{0.5}MnO_3$ compound shows remarkable electronic and magnetic properties. As it is cooled below the Curie temperature ($T_C \approx 270$ K in Ref. 6), the electrical resistivity (ρ) shows a noticeable drop due to the suppression of spin-flip scattering.[6] Upon further cooling, a sharp upward discontinuity in the ρ vs T data occurs near 140 K, below which the resistivity continues to increase. This discontinuity is reminiscent of a metal-insulator transition. Tomioka *et al.* first suggested that this transition is due to the onset of

charge ordering. The application of an external magnetic field drove T_{co} down, eventually "melting" the charge-ordered state completely for $\mu_0 H \approx 7$ T and reestablishing the metallic state.[6] However, a neutron diffraction study of $Pr_{0.5}Sr_{0.5}MnO_3$ showed that there was no clear indication of charge ordering[12] and that the phase transition at 140 K is due to the formation of an A-type antiferromagnetic (AFM) structure. Therefore, we will refer to the magnetic phase transition from ferromagnetic (FM) to AFM as occurring at the Néel temperature (T_N). Similarly, neutron diffraction results by Damay *et al.* show no evidence of charge ordering near T_N.[13] They also show that the crystal structure of the FM phase (tetragonal; space group $I4/mcm$) changes to orthorhombic (space group $Fmmm$) near T_N. The onset of this A-type AFM structure correlates well in temperature with the feature in their ρ vs T data near 140 K, consistent with the observation of a metal-insulator transition at this temperature.

It should be pointed out that metallic behavior in ρ vs T above $T_N \approx 140$ K was observed in single crystals reliably,[6] whereas data on polycrystalline $Pr_{0.5}Sr_{0.5}MnO_3$ showed approximately exponential activation above T_N.[14] Chen *et al.* observed a large change in entropy near 161 K in polycrystalline $Pr_{0.5}Sr_{0.5}MnO_3$ by means of measurement of magnetization (M) as a function of temperature.[7] The change in entropy of 7.1 J/kg K near T_N is positive and much greater than the values measured near T_C. Chen *et al.* suggested that this large change in entropy at 161 K is due to a magnetic phase transition from FM to AFM states occurring concomitantly with an abrupt change in lattice parameters.[14] It should be noted, when comparing the entropy of CMR materials, that care must be taken to consider the moderating effect of heat capacity, which can be large.[15]

Crystallographic changes accompanying a metal-insulator transition in $R_{1-x}A_x MnO_3$ materials frequently result in interactions leading to electrical behavior that depends strongly on temperature and pressure (P).[16] The exact nature of these interactions is often highly dependent on composition and structure. In addition, the electronic and magnetic properties

are frequently related to the Mn-O-Mn bond angle in the perovskite structure.[17] Substitution of variously sized ions serves to distort the lattice structure and, consequently, bond angles, while also affecting the available charge carrier concentration. On the other hand, hydrostatic pressure can affect the lattice without the introduction of disorder. However, since the compressibility is anisotropic, the application of pressure results in the elongation of MnO_6 octahedra along the c axis, decreasing the average Mn-O bond length and straightening the Mn-O-Mn angle.[18] A pressure study of ρ vs T in polycrystalline $Pr_{0.5}Sr_{0.5}MnO_3$ showed a depression of the resistivity below T_N in pressures of up to 1.4 GPa.[19] Previous work has shown some variance in ρ vs T both in single crystal and polycrystalline samples.[13,14,19] The metal-insulator transition feature in ρ vs T at T_N is more gradual in the polycrystalline material,[13] and the onset of the FM metallic state is less pronounced,[19] or not observed.[14] In single crystals, both the metal-insulator transition in the ρ vs T data and the metallic conductivity of the FM state for $T_N < T < T_C$ can be clearly observed.[6,12,20] Grain boundary effects in polycrystalline specimens may explain the differences seen in the ρ vs T data as compared to the data in single crystals.

In order to determine the effect of hydrostatic pressure on the transport properties of $Pr_{0.5}Sr_{0.5}MnO_3$, we carried out measurements of the electrical resistivity vs temperature in a single-crystalline specimen.

II. EXPERIMENTAL DETAILS

The precursor material for the crystal growth process was synthesized by solid-state reaction. Stoichiometric amounts of high purity Pr_6O_{11}, $SrCO_3$, and MnO_2 were weighed and ground together thoroughly. The mixture was placed in an alumina crucible, and reacted at 1200 °C for 22 h in air. The sample was reground and annealed again at 1200 °C for 43 h. The resulting powder was pressed into 5 mm diameter cylinders, which were used for the crystal growth in an optical furnace. The top and bottom stubs were rotated in opposing directions at 50 rpm, while the molten zone was swept at the rate of 7 mm/h, resulting in a 38 mm long single crystal. This growth was carried out in air at ambient pressure, after which the sample was annealed for 33 h at 1250 °C in air, and cooled to room temperature (RT) at the rate of 0.5 °C/min. We examined samples from three cuts, located 2 mm (cut 1), 15 mm (cut 2), and 39 mm (cut 3) from the seed end. Powder x-ray diffraction (XRD) analysis showed that the samples from the three cuts were single phase, and the presence of impurity phases could not be detected. However, the sample from cut 3 had the best Rietveld match to the $I4/mcm$ ideal structure, yielding lattice parameters $a=5.4077$ Å and $c=7.7760$ Å. The Mn-O bond lengths and Mn-O-Mn bond angles for the samples from the three cuts are consistent with the values obtained from powder neutron diffraction;[18] however, any variation between the three cuts could not be resolved within the accuracy of our refinements. The larger discrepancies between the calculated and measured intensities in the XRD histograms in the samples from cuts 1 and 2 suggest that they may have non-ideal stoichiometry. Actually, albeit the large uncertainties, a

semiquantitative microprobe analysis suggested that the Pr:Sr concentration ratio decreased slightly during the growth, being the closest to 1.0 for the sample from cut 3.

Magnetic susceptibility (χ) and magnetization measurements in the 1.9–400 K range were conducted with the vibrating sample magnetometer option of a Quantum Design physical property measurement system (PPMS-9). Specific heat (C_p) measurements on a 2.7 mg piece of the crystal (cut 3) were carried out in the 1.9–300 K temperature range using a relaxation technique, in the PPMS-9 as well. Resistance measurements were carried out in the temperature range of 10–300 K with a linear research LR-400 four-wire bridge using a close-cycle helium refrigerator.

The measurements of ρ vs T in hydrostatic pressures up to 2 GPa were carried out in a self-locking piston-cylinder pressure cell. Four platinum leads were attached to the sample with silver epoxy, and the sample was mounted at the high-pressure end of a feedthrough, close to a coil of manganin which served as a manometer at room temperature. This assembly was then placed inside of a Teflon capsule filled with Fluorinert FC-75, which was used as the pressure transmitting medium, and the cell was sealed. The value of the pressure at RT was monitored with the manganin manometer. Force was applied using a hydraulic press and the pressure was locked in at RT. The small reduction in cell pressure with temperature, which is typical for this type of cell,[21] was estimated both from the changes in resistance of the manganin manometer with T and from a previous characterization of the pressure loss using the superconducting transition temperature of Sn as a reference. The temperature of the sample was monitored with a Si diode placed on the beryllium-copper body of the cell. The cell was first cooled from RT to 10 K at a rate of ≈ 2.5 K/min. The ρ vs T data were collected while the cell was slowly warmed up from 10 to 300 K. In order to reduce the lag in temperature between the sensor and the sample, data between 10 and 50 K were acquired with the refrigerator on, while a heater provided just enough power to raise the temperature of the cell at a rate of $\leqslant 0.5$ K/min. Measurements above 50 K were taken with the refrigerator and heater off, while the cell warmed naturally at a rate of $\leqslant 0.5$ K/min. The lag in temperature between the sample and the sensor was estimated to be below 0.2 K throughout the temperature range of the experiment.

III. EXPERIMENTAL RESULTS

The temperature dependence of the electrical resistivity for samples from the three cuts at zero applied pressure is shown in Fig. 1. As the temperature is lowered, samples of all three cuts show a drop in resistivity near T_C, which varied between the three samples from 255 to 290 K, below which the resistivity continues to decrease. The drop in resistivity near T_C is consistent with the suppression of spin-flip scattering due to the onset of FM order. The ρ vs T data for cut 3 show a clear metal-insulator transition at $T_N \approx 161$ K. In order to carry out a systematic characterization of the effect of pressure, we took both transition temperatures, T_C and T_N, from the peaks in the derivative $d\rho/dT$. There is a significant
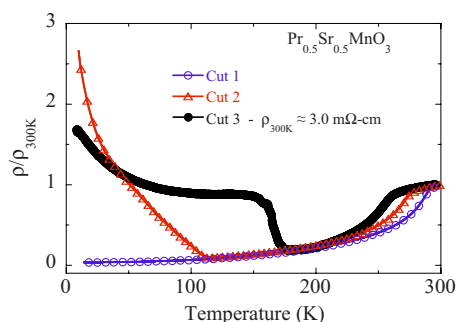
FIG. 1. (Color online) Normalized electrical resistivity $\rho/\rho_{300\,K}$ vs T for samples from the three cuts of the $Pr_{0.5}Sr_{0.5}MnO_3$ single crystal. The drop in ρ near 255 K (cut 3) is due to the onset of ferromagnetism, while a metal-insulator transition can be observed near 161 K. For clarity, only a partial number of data points is shown. The solid lines are guides for the eyes.

variance in the determination of T_N for these compounds in the literature, possibly reflecting how strongly dependent the crystallographic, electronic, and magnetic properties are to subtle changes in composition. For example, the low temperature transitions in single crystals are given as 114,[6] 150,[12] and 155 K,[20] while the value of $T_N \approx 161$ K in a polycrystal (Ref. [7]) matches the value for the single crystal of our work. The remarkable difference in behavior between samples, even from the three cuts of the same crystal, underscores how sensitive the electronic properties are to composition. Comparison with the ρ vs T data in Ref. [20] suggests that the Pr:Sr ratio of cut 1 sample may be close to 0.48:0.52. In light of the better structural and compositional properties of cut 3, we chose it for our pressure studies, as well as for the measurement of magnetization and specific heat.

Measurements of the M vs T for $\mu_0 H = 0.5$ T in cut 3 specimen are shown in Fig. 2. These data show typical FM behavior slightly below room temperature, as well as the onset of the AFM phase at ≈ 161 K. The feature in M vs T at T_N coincides in temperature with the metal-insulator transition seen in the ρ vs T data of Fig. 1. The inset of Fig. 2 shows a plot of χ^{-1} vs T for 200 K $< T <$ 400 K. The value of χ above T_C, in this case, for 300 K $\leqslant T \leqslant$ 400 K, could be fit

to a Curie-Weiss expression, $\chi = \chi_0 + C/(T-\theta)$, yielding $\theta \approx 265$ K. The value of the effective magnetic moment extracted from the χ^{-1} vs T data above 350 K is $\mu_{eff} = 5.56\mu_B$. Assuming that the contribution of Pr^{3+} to this value is $3.58\mu_B$/ion, the average value of the effective moment for each Mn ion is $3.77\mu_B$, slightly lower than the $2[S(S+1)]^{1/2}$ value of $3.87\mu_B$ for Mn^{4+}.

The magnetization curves for this sample are shown in Fig. 3. The isotherms of M vs $\mu_0 H$ clearly reflect the onset of FM order as the temperature is reduced from 300 to 250 K. Below T_N, the magnetization curves at $T = 20$, 100, and 150 K clearly show that a metamagnetic transition takes place and that the spin realignment field is inversely correlated to the temperature. The hysteretic nature of the metamagnetic transition suggests that the phase transformation from the FM to AFM phase has a first order character.

The temperature dependent specific heat $C_p(T)$ data for cut 3 sample are shown in Fig. 4, where two remarkable features can be identified: (1) a peak is seen near 260 K, consistent with the onset of magnetic ordering at T_C, and (2) a double-peak feature is observed slightly below T_N. As shown in the inset, the effect of a magnetic field $\mu_0 H = 1$ T is to shift this feature near T_N to lower temperatures, therefore extending the T range of the FM order. In light of the M vs

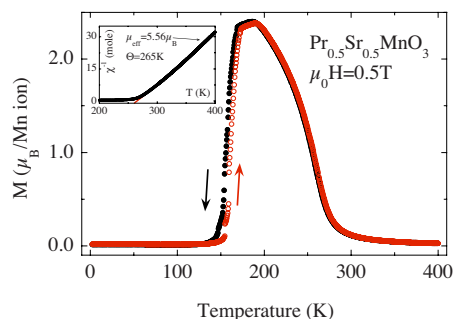FIG. 2. (Color online) Magnetization vs temperature in $\mu_0 H = 0.5$ T for $Pr_{0.5}Sr_{0.5}MnO_3$ (cut 3). The inset shows a plot of χ^{-1} vs T at high temperatures. A fit of the χ^{-1} vs T data to the Curie-Weiss law for 300 K $\leqslant T \leqslant$ 400 K yields a Curie-Weiss temperature $\Theta \approx 265$ K. The effective moment yielded from the $\chi^{-1}(T)$ data for $T \geqslant 350$ K is $\mu_{eff} \approx 5.56\mu_B$.
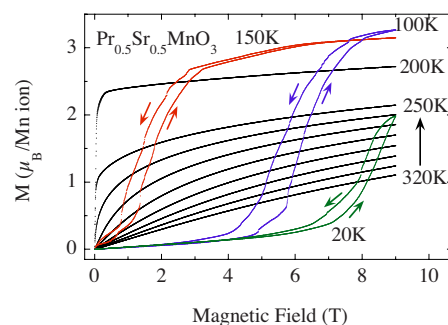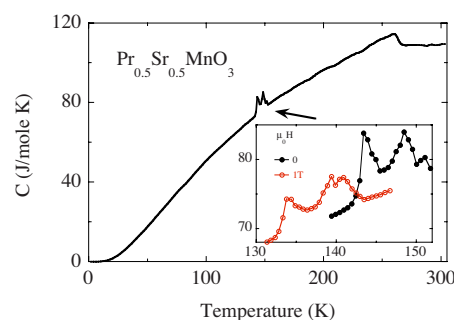

FIG. 3. (Color online) Magnetization curves for $Pr_{0.5}Sr_{0.5}MnO_3$ (cut 3) for 320 K $\leqslant T \leqslant$ 20 K in magnetic fields of up to 9 T. The isotherms between 250 and 320 K are spaced by 10 K. The M vs $\mu_0 H$ curves below T_N show spin realignment behavior, consistent with the occurrence of a metamagnetic transition. The hysteretic behavior of the latter is reminiscent of first order phase transitions.

FIG. 4. (Color online) Specific heat vs temperature for $Pr_{0.5}Sr_{0.5}MnO_3$ (cut 3). The feature near 260–266 K is due to the onset of FM order, while the double-peak feature centered near 146 K is due to the AFM-FM phase transformation. The latter phase change is shifted to lower temperatures in magnetic field (see inset).
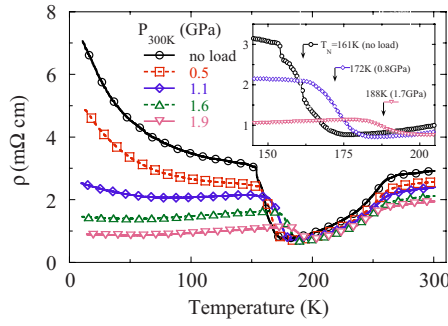
FIG. 5. (Color online) Quasi-isobaric measurements of ρ vs T in pressures of up to 2.0 GPa. For clarity, only a small number of data points is shown. The inset shows the detailed behavior of ρ vs T near the metal-insulator transition for $P \approx 0$ (no load), 0.8, and 1.7 GPa. The values of T_N were determined from the peak in $d\rho/dT$. The P values in the inset are corrected to account for the change in pressure with the cell temperature.

H data of Fig. 3, showing that the elbow of the metamagnetic transition at 150 K is close to 1 T, the same field of the $C_p(T)$ data of Fig. 4 (inset), the partial suppression of the double-peak feature in $C_p(T)$ near T_N for $\mu_0 H = 1$ T is consistent with a field-induced reduction in magnetic entropy.

The temperature dependence of the electrical resistivity of cut 3 sample was examined in hydrostatic pressures of up to 2 GPa. The ρ vs T data for several nominal pressures at room temperature are shown in Fig. 5. The FM transition temperature near 255 K (value taken from a maximum in $d\rho/dT$ near the transition) drops gradually with pressure, reaching ≈ 249 K at ≈ 1.9 GPa. Below T_C, the crystal enters a FM state, where the resistivity drops with pressure as well as with cooling, as shown in Fig. 5. A transition from FM metal to AFM insulator is seen at $T_N \approx 161$ K for the no-load measurement in the pressure cell. The application of pressure shifts this transition to higher temperatures in an almost linear fashion, increasing it from ≈ 161 K (no load) to ≈ 188 K for $P \approx 1.7$ GPa. The pressure dependence of the transition temperatures T_N and T_C is plotted in Fig. 6(a), where the contours of the magnetic phase diagram are delineated. The effect of pressure on the change in resistivity at the FM-AFM phase boundary is plotted Fig. 6(b). These data suggest that the metal-insulator transition could be completely suppressed at $P \approx 2.4$ GPa.

Isotherms of ρ vs P are shown in Fig. 7. The ambient temperature electrical resistivity decreases approximately linearly as pressure is increased from 0 to 2 GPa. The effect of pressure on the resistivity is much stronger below T_N, where upon the suppression of the AFM phase in favor of FM, the metallic state is recovered. For example, the value of $d\rho/dP$ changes from about -0.5 mΩ cm/GPa at 300 K to -1.3 and -1.9 mΩ cm/GPa at 100 and 50 K, respectively, reflecting the gradual suppression of the AFM insulating state and promotion of the conducting FM phase.

IV. DISCUSSION

In order to understand the decrease of ρ and the suppression of the metal-insulator (or equivalently FM-AFM) tran-
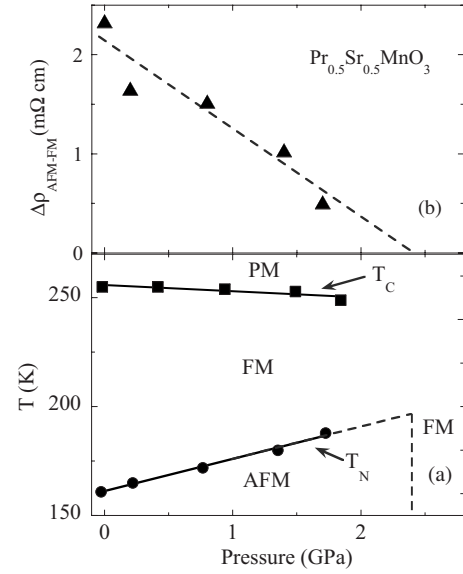

FIG. 6. (a) Magnetic phase diagram and pressure dependence of T_C and T_N. The values of T_C and T_N were taken from the maxima in $d\rho/dT$ near the transitions. The dashed line is a qualitative estimate of the phase diagram for $P > 2.0$ GPa; (b) Effect of pressure on the change in $\Delta\rho$ at the AFM-FM transition, suggesting that the AFM phase could be suppressed near 2.4 GPa.

sition at T_N with pressure in $\mathrm{Pr}_{0.5}\mathrm{Sr}_{0.5}\mathrm{MnO}_3$, we need to examine the effect of pressure on the lattice and on the magnetic order. The effect of pressure on the lattice is to reduce the Mn-O bond lengths both in the FM-$I4/mcm$ and the AFM-$Fmmm$ phases, while straightening the Mn-O-Mn angles above T_N and decreasing them below.[18] The sharp increase in ρ near T_N was observed to diminish with pressure both in a single crystal (this work) as well as in a polycrystalline material.[19] However, while pressure gradually drives ρ vs T data below T_N toward metallic behavior in the single crystal, the polycrystalline material shows nonmetallic behavior in pressures of up to 1.4 GPa,[19] perhaps underlining the contribution of the grain boundaries to the transport properties.

A neutron powder diffraction study of $\mathrm{Pr}_{0.5}\mathrm{Sr}_{0.5}\mathrm{MnO}_3$ under pressure reveals the gradual transformation of the AFM-$Fmmm$ phase into the FM-$I4/mcm$ phase below T_N.[18]
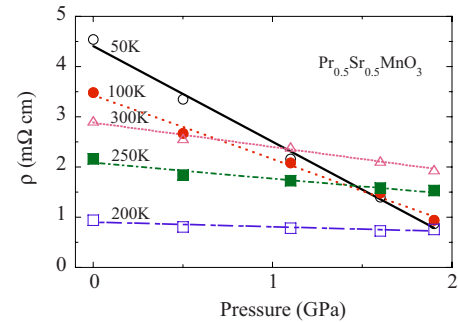

FIG. 7. (Color online) Isotherms of ρ vs P for $\mathrm{Pr}_{0.5}\mathrm{Sr}_{0.5}\mathrm{MnO}_3$ in pressures ($P_{300\,K}$) up to 2 GPa. The magnitude of $d\rho/dP$ below T_N is three to four times higher than above it, reflecting the suppression of the insulating AFM phase in favor of the metallic FM phase.

It is argued that the metal-insulator transition results from the AFM superexchange interactions winning over the double-exchange mechanism of the FM state at T_N.[18] The effect of pressure below T_N is then to promote the tetragonal (FM) phase at the expense of the orthorhombic (AFM) phase. At the same time, a decrease in the interionic distances due to pressure possibly strengthens the superexchange interaction, therefore shifting the onset of the AFM phase to higher temperatures, and increasing T_N, as observed in this work. With successive gains in pressure, the FM/AFM phase ratio increases, and the discontinuity in ρ at T_N is gradually suppressed. Extrapolation of the $\Delta\rho$ vs P data near T_N suggests that the metal-insulator transition can be completely suppressed for $P \approx 2.4$ GPa. The effect of pressure on the electronic density of states (DOS) must also be considered. The DOS has been shown to vary with temperature across both T_N and T_C in epitaxial films of $Pr_{0.5}Sr_{0.5}MnO_3$.[22] The highest DOS of the FM phase is consistent with the higher electrical conductivity. The inducement of the FM phase below T_N by pressure is therefore accompanied by the suppression of the crystallographic transformation, and an increase of the DOS at the Fermi level, consistent with the more metallic behavior of ρ vs P under pressure.

It has been shown that the conductivity in perovskites increases as the Mn-O-Mn bond angle is straightened.[17] From a structural point of view, it is tempting to consider that the improvement in conductivity with pressure above T_N is correlated both to the shortening of the Mn-O bond lengths and the straightening of the Mn-O-Mn angles. However, the effect of pressure below T_N is more complex. The Mn-O bond lengths expand and the Mn-O-Mn angles are reduced as the material transitions from the FM to the AFM phase, yielding to a less conducting state. The effect of pressure is twofold. First, it suppresses this transition, leading to a more conducting state. Second, the Mn-O bond lengths of the residual AFM regions of the mixed phase regime ($P < 2.4$ GPa) are reduced by pressure,[18] leading to an enhancement of the superexchange interaction and to an increase in T_N.

Similar to our results, the effect of pressure on ρ vs T for polycrystalline $Pr_{0.5}Sr_{0.5}MnO_3$ showed an increase in T_N; however, T_C was left nearly unaffected.[19] It is important to notice that extrinsic effects due to the presence of grain boundaries in polycrystalline materials broaden the transitions considerably, which complicates the analysis of the results. In contrast to the data for the polycrystalline material,[19] the sharper features of the ρ vs T data at T_N and T_C in the single crystal permit a much more reliable determination of the effect of pressure on T_N and T_C. The values of dT_N/dP and dT_C/dP for the single crystal of this work are ≈ 14.2 and -3.2 K/GPa, respectively, and the ρ vs T data of Fig. 5 clearly suggest that pressure suppresses the AFM phase in favor of the FM phase.

The double-peak feature in the C_p vs T data correlates well in temperature with the AFM-FM phase transition. It is tempting to ascribe this double-peak character of this feature, i.e., the ≈ 5 K separation between the two peaks, to the crystallographic and magnetic phase transformations taking place at slightly different temperatures. However, this point will require further investigation. The full shift of this feature with magnetic field suggests that it is intrinsic. The ≈ 10 K shift of the double-peak feature at T_N to lower temperatures for $\mu_0 H = 1$ T is consistent with the magnetoresistance data in Ref. 6, in which the resistive anomaly at T_N is shifted down in temperature by the same amount, suggesting that the effect of the magnetic field is to drive the spin realignment transition and the crystallographic transformation to lower temperatures.

V. SUMMARY

In summary, we have investigated the magnetic, thermal, and electrical transport properties of single-crystalline $Pr_{0.5}Sr_{0.5}MnO_3$, the latter in hydrostatic pressures of up to 2 GPa. It is well established that the FM order at $T_C \approx 255$ K is mediated by a double-exchange mechanism, while superexchange interactions lead to an AFM order at $T_N \approx 161$ K. The effect of pressure is to depress T_C and increase T_N at the respective rates of ≈ -3.2 and 14.2 K/GPa. Although the value of T_N increases with pressure, due to the shortening of the Mn-O bonds, and resulting enhancement of the superexchange interaction, the AFM-$Fmmm$ state is progressively suppressed, as pressure stabilizes the FM-$I4/mcm$ phase to lower temperatures. Extrapolation of our $\Delta\rho$ vs P data with pressure at T_N suggests that the AFM phase should be completely suppressed near 2.4 GPa. In light of the complex interrelation between the crystallographic and magnetic interactions in this compound, studies at higher pressures are in order. Similarly, the nature of the double-peak feature in the C_p data near T_N needs to be clarified.

ACKNOWLEDGMENTS

*Present address: Department of Physics, University of Connecticut, Storrs, CN 06269-3046.

[1] R. von Helmolt, J. Wecker, B. Holzapfel, L. Schultz, and K. Samwer, Phys. Rev. Lett. **71**, 2331 (1993).

[2] K. Chahara, T. Ohno, M. Kasai, and Y. Kosono, Appl. Phys. Lett. **63**, 1990 (1993).

[3] J. Goodenough, Phys. Rev. **100**, 564 (1955).

[4] Z. B. Guo, J. R. Zhang, H. Huang, W. P. Ding, and Y. W. Du, Appl. Phys. Lett. **70**, 904 (1997).

[5] T. Tang, K. M. Gu, Q. Q. Cao, D. H. Wang, S. Y. Zhang, and Y. W. Du, J. Magn. Magn. Mater. **222**, 110 (2000).

[6] Y. Tomioka, A. Asamitsu, Y. Moritomo, H. Kuwahara, and Y. Tokura, Phys. Rev. Lett. **74**, 5108 (1995).

[7] P. Chen, Y. W. Du, and G. Ni, Europhys. Lett. **52**, 589 (2000).

[8] H. L. Wang, G. S. Tian, and H. Q. Lin, Commun. Theor. Phys. **43**, 179 (2005).

[9] P. G. DeGennes, Phys. Rev. **118**, 141 (1960).

[10] C. Zener, Phys. Rev. **82**, 403 (1951).

[11] P. W. Anderson and H. Hasegawa, Phys. Rev. **100**, 675 (1955).

[12] H. Kawano, R. Kajimoto, H. Yoshizawa, Y. Tomioka, H. Kuwahara, and Y. Tokura, Phys. Rev. Lett. **78**, 4253 (1997).

[13] F. Damay, C. Martin, M. Hervieu, A. Maignan, B. Raveau, G. André, and F. Bourée, J. Magn. Magn. Mater. **184**, 71 (1998).

[14] K. Knizek, Z. Jirák, E. Pollert, and F. Zounova, J. Solid State Chem. **100**, 292 (1992).

[15] H. Terashita, J. J. Garbe, and J. J. Neumeier, Phys. Rev. B **70**, 094403 (2004).

[16] H. Y. Hwang, T. T. M. Palstra, S. W. Cheong, and B. Batlogg, Phys. Rev. B **52**, 15046 (1995).

[17] J. B. Torrance, P. Lacorre, A. I. Nazzal, E. J. Ansaldo, and C. Niedermayer, Phys. Rev. B **45**, 8209 (1992).

[18] D. P. Kozlenko, V. P. Glazkov, Z. Jirák, and B. N. Savenko, J. Phys.: Condens. Matter **16**, 2381 (2004).

[19] I. V. Medvedeva, C. Martin, Y. S. Bersenev, V. Morshchakow, K. Bärner, and B. Raveau, Phys. Met. Metallogr. **97**, 169 (2004).

[20] E. Pollert, Z. Jirák, J. Hejtmánek, A. Strejc, R. Kuzel, and V. Hardy, J. Magn. Magn. Mater. **246**, 290 (2002).

[21] J. D. Thompson, Rev. Sci. Instrum. **55**, 231 (1984).

[22] B. C. Yao, J. B. Lee, C. C. Chi, M. K. Wu, and H. C. Yang, J. Magn. Magn. Mater. **209**, 103 (2000).